++Supporting information++

New and Facile Preparation Method for Highly Active Iron Oxide Catalysts for CO Oxidation

Steffen Schlicher[1], Roland Schoch[1,*], Nils Prinz[2], Mirijam Zobel[2] and Matthias Bauer[1]

[1] Department of Chemistry and Center for Sustainable Systems Design (CSSD), Paderborn University, Warburger Straße 100, 33098 Paderborn, Germany; matthias.bauer@upb.de (M.B.)

[2] Insitute of Crystallography, RWTH Aachen University, Jägerstraße 17-19, 52066 Aachen, Germany;; zobel@ifk.rwth-aachen.de (M.Z.)

[*] Correspondence: roland.schoch@upb.de

Powder diffraction 2

PDF analysis 3

DRUVS 5

SEM 6

XAS 9

Catalytic tests 17

Powder diffraction

Due to a shift of diffraction reflexes to lower Q-values/Bragg angles with higher Fe-loadings, the corresponding lattice parameters *a* for the different loadings were calculated and plotted for the 440 lattice. This reflex was chosen because of its high intensity and the absence of overlap with other reflexes. A linear correlation according to Vegard's law is recognizable, as can be seen in Figure S1.

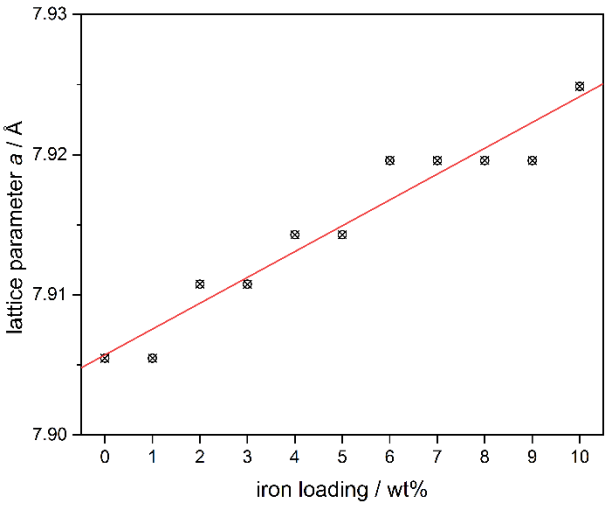


Figure S1: Lattice parameter a calculated from PXRD reflexes of the lattice planes (440) calculated for the catalysts FE01 - FE10 and the pure support material and their linear fit.

To elucidate the nature of the Fe_2O_3 on the support, a qualitative approach was used: a calculated powder pattern of a 2.5 nm γ-Fe_2O_3 nanoparticles (solid black line; using Scherrer equation for FWHM of the pattern) was added to the unloaded support (red line), see Figure S2. The sum (dashed line) fits the experimental powder pattern of FE09 (green line) rather good, which leads to the assumption that there are Fe_2O_3 nanoparticles of very small size present in the sample. Further isolated iron sites cannot be excluded by this and are very probable as shown by XAS.

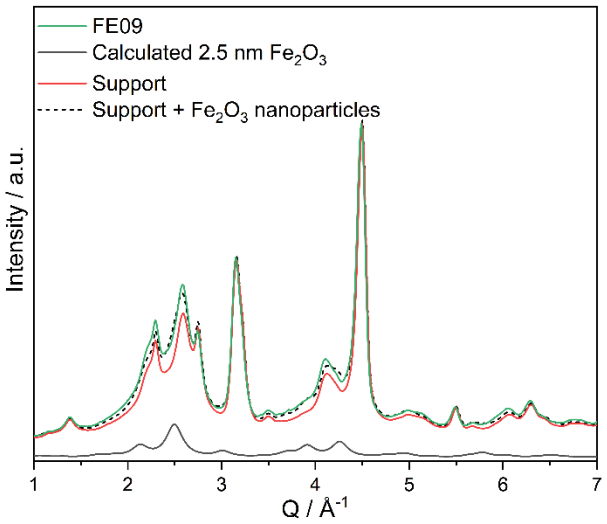


Figure S2: Estimation of 2.5 nm Fe_2O_3 nanoparticles in the PXRD of FE09.

The diffraction patterns of MI01-MI10 do only show reflexes corresponding to the γ-alumina support material, indicating amorphous iron species. The diffractogram of SI10 exhibits small reflexes, which can be assigned to a mixture of α- and γ-Fe_2O_3 (see Figure S3).

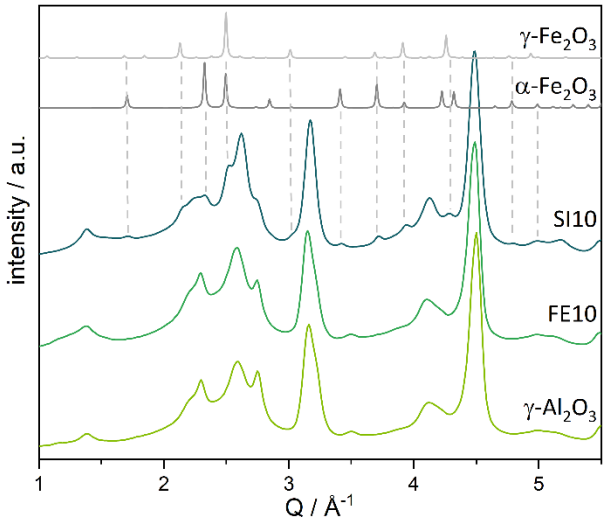


Figure S3: Comparison of FE10 and SI10 with pure γ-alumina and α-Fe_2O_3 (calculated) as references

PDF analysis

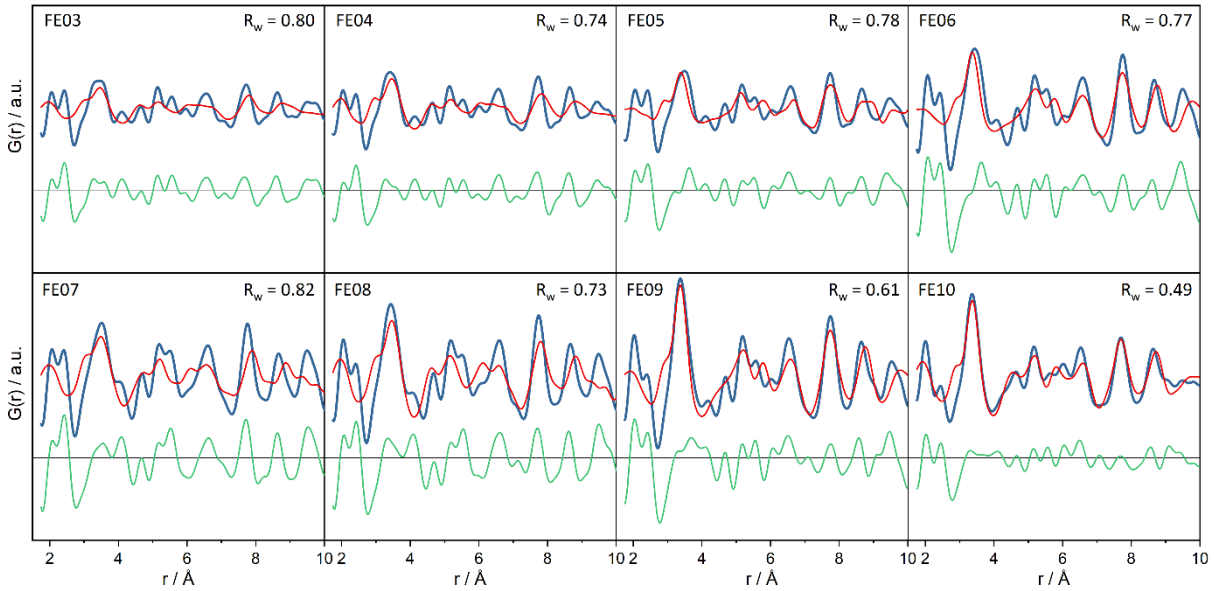


Figure S4: dPDF refinements from impregnation step 3 to 10 using a γ-Fe_2O_3-model. Up to MI08 the high R_w value shows that the structure is not well described by the crystalline γ-Fe_2O_3. For MI10 the crystalline model fits well, except for the missing distance at 2.97 Å.

dPDF refinements were carried out starting with a γ-Fe_2O_3-model. According to the obtained R_w values, the structures of the catalysts cannot be described well using crystalline γ-Fe_2O_3 up to FE08. For FE09 and FE10 the R_w value decreases significantly, since except one contribution at 2.97 Å the spectrum can be fitted very well with this γ-Fe_2O_3 structural model. Therefore, a higher amount of crystalline nanoparticles at loadings FE09 and FE10 can be deduced.

Table S1: Fit results of the dPDF refinement parameters of the samples FE03-FE10 and literature values of bulk γ-$Fe_2O_3$for comparison

Sample	Refinement parameter				
	Lattice parameter *a*	B_{iso} *(O)*	B_{iso} *(Fe)*	δ_2	R_w
FE03	8.304 Å	0.0 Å^2	3.7 Å^2	0.0	0.80
FE04	8.227 Å	0.1 Å^2	2.1 Å^2	0.0	0.74
FE05	8.280 Å	0.1 Å^2	2.5 Å^2	0.0	0.78
FE06	8.296 Å	0.2 Å^2	2.6 Å^2	0.0	0.77
FE07	8.344 Å	0.1 Å^2	2.8 Å^2	0.0	0.82
FE08	8.293 Å	0.2 Å^2	2.5 Å^2	0.0	0.73
FE09	8.128 Å	7.6 Å^2	1.1 Å^2	0.5	0.61
FE10	8.097 Å	2.6 Å^2	1.0 Å^2	0.0	0.49
Bulk γ-Fe_2O_3*	8.347 Å	0.5 Å^2	0.5 Å^2	-	-

*: A. N. Shmakov, G. N. Kryukova, S. V. Tsybulya, A. L. Chuvilin, L. P. Solovyeva, *J Appl Crystallogr* **1995**, *28*, 141–145.

The lattice parameter *a* for the 10th impregnation sample FE10 is 0.25 Å smaller than the literature value for bulk γ-Fe_2O_3 (for comparison, see Figure S4 and Table S1). This contraction stems from the nano-size of our synthesized catalyst. For FE03 – FE08 the lattice parameter is closer to the bulk value, but in light of the high R_w value (and the very high B_{iso}(Fe)), this needs to be interpreted with care. These high R_w values show that the iron oxide species cannot simply be described by the crystalline γ-Fe_2O_3 structure. Instead, disorder is present either in the particles or at the γ-Al_2O_3/γ-Fe_2O_3 interface, because of Fe^{3+} introduction into the defective spinel structure of γ-Al_2O_3. The result would be a

defective $FeAl_2O_4$ type spinel, which would also explain the subtle observed shifts of the Bragg reflections of γ-Al_2O_3 in the PXRD pattern, as the introduction of Fe^{3+} widens up the crystal lattice.

DRUVS

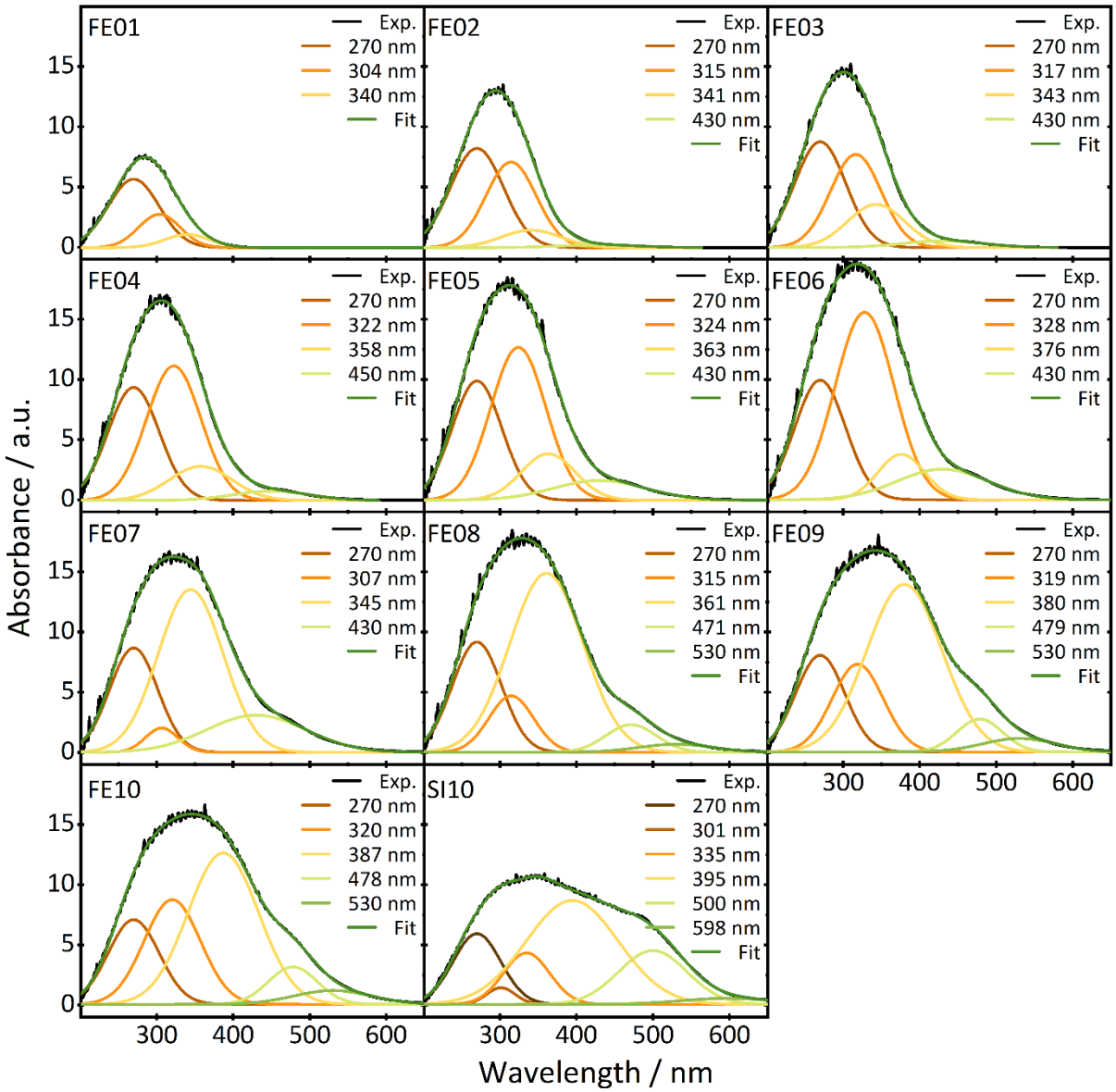


Figure S5: DRUV spectra of catalysts FE01 - FE10 and SI10 and resulting peak deconvolution with the respective peak centers and their convoluted fit.

SEM

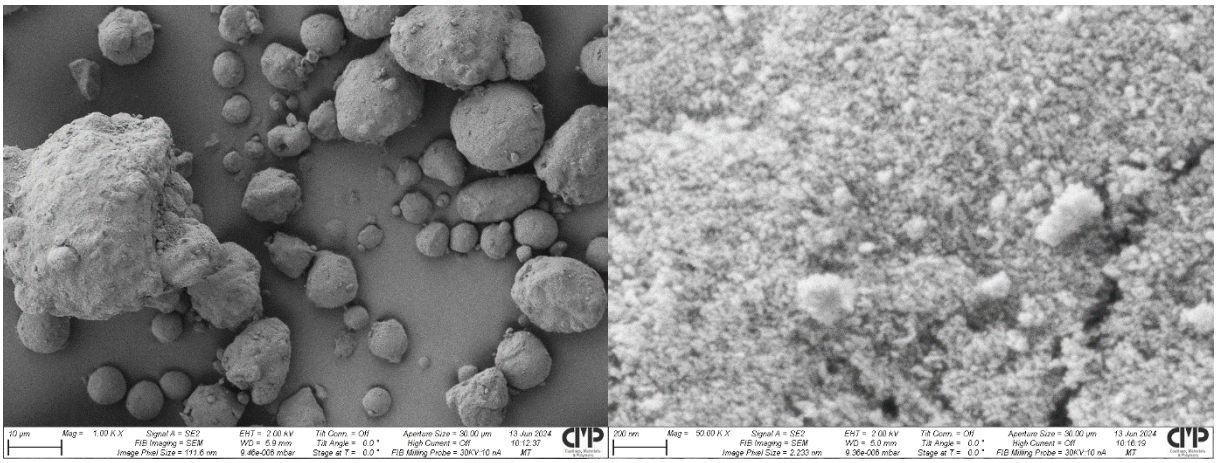


Figure S6: SEM pictures of FE01 in 1 000 fold (left) and 50 000 fold magnification (right).

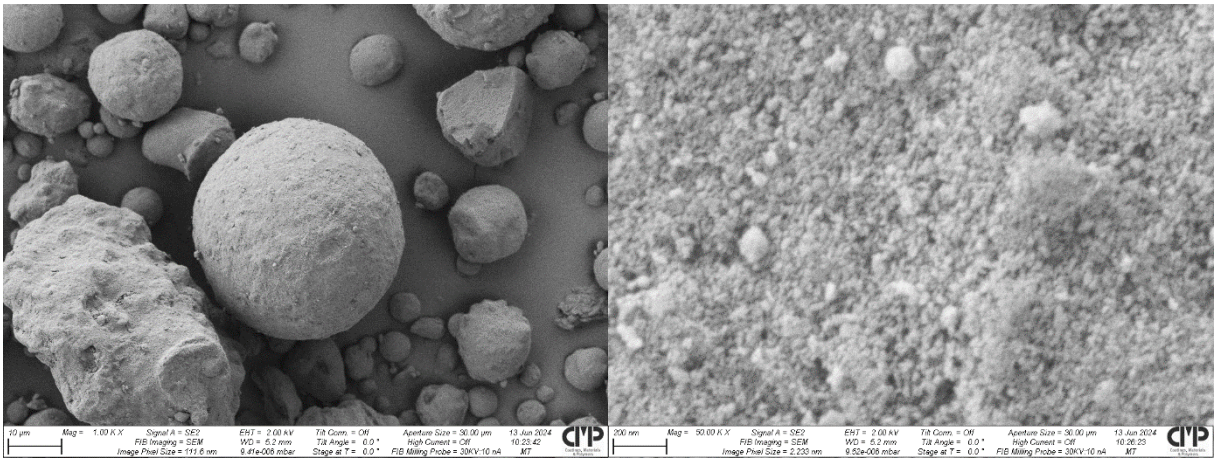


Figure S7: SEM pictures of FE03 in 1 000 fold (left) and 50 000 fold magnification (right).

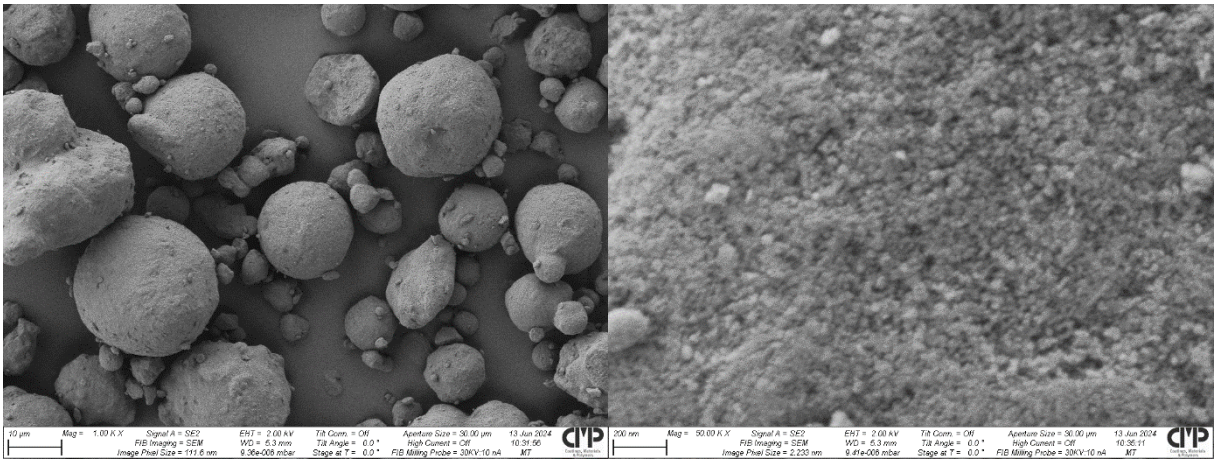


Figure S8: SEM pictures of FE05 in 1 000 fold (left) and 50 000 fold magnification (right).

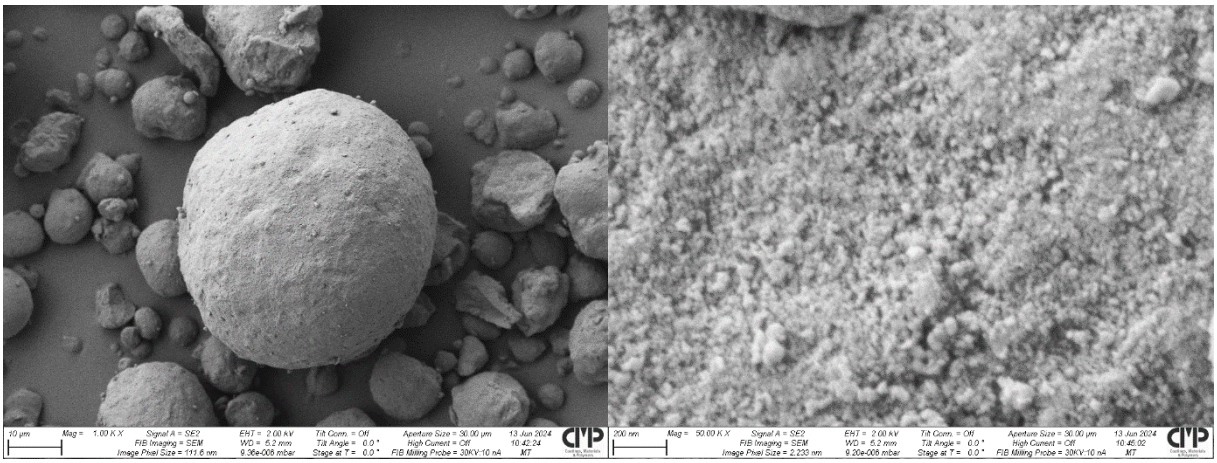


Figure S9: SEM pictures of FE07 in 1 000 fold (left) and 50 000 fold magnification (right).

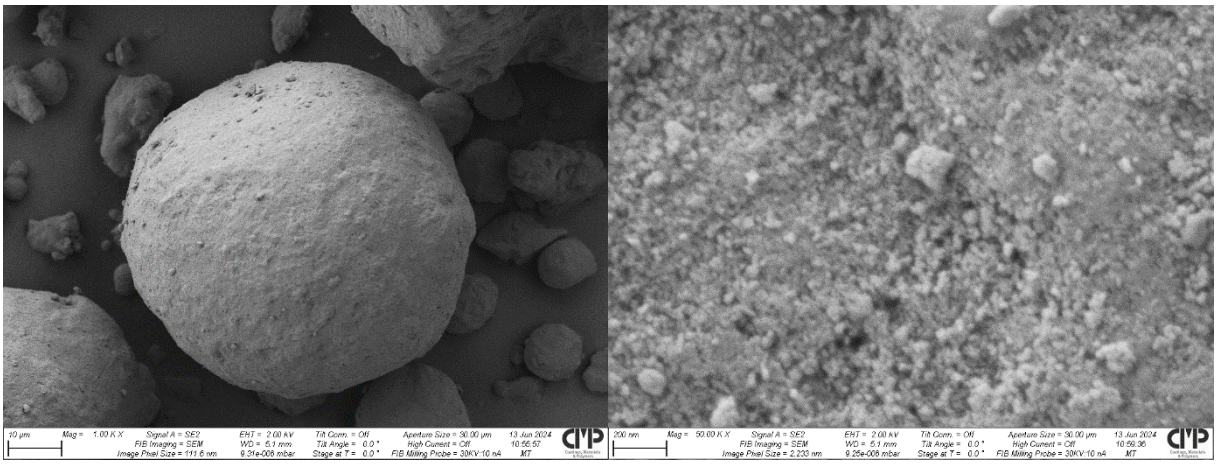


Figure S10: SEM pictures of FE08 in 1 000 fold (left) and 50 000 fold magnification (right).

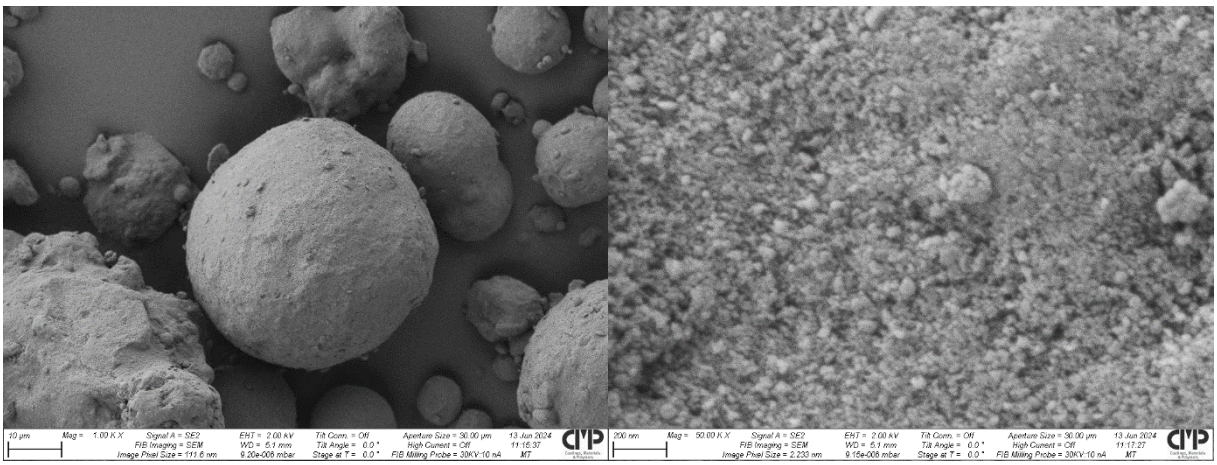


Figure S11: SEM pictures of FE09 in 1 000 fold (left) and 50 000 fold magnification (right).

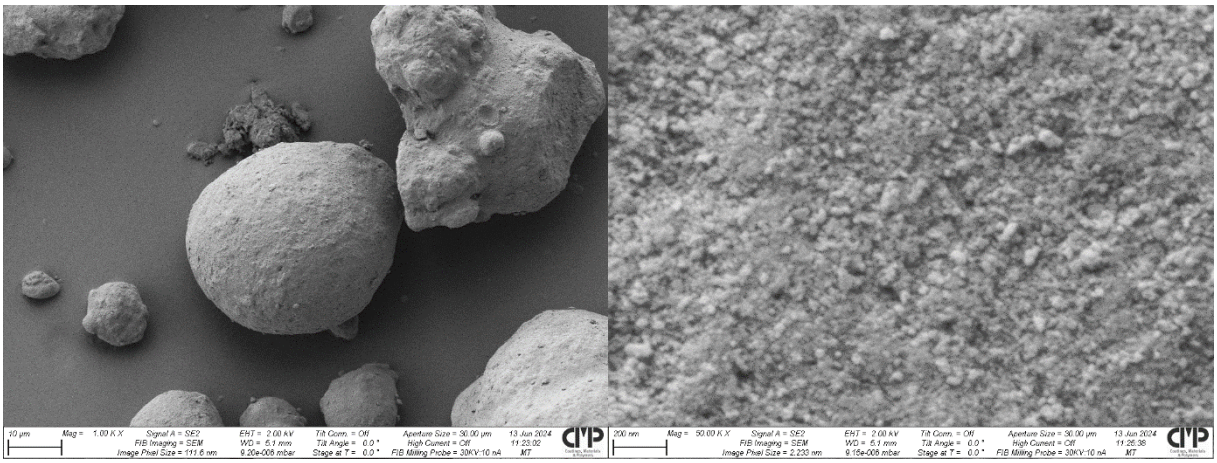


Figure S12: SEM pictures of FE10 in 1 000 fold (left) and 50 000 fold magnification (right).

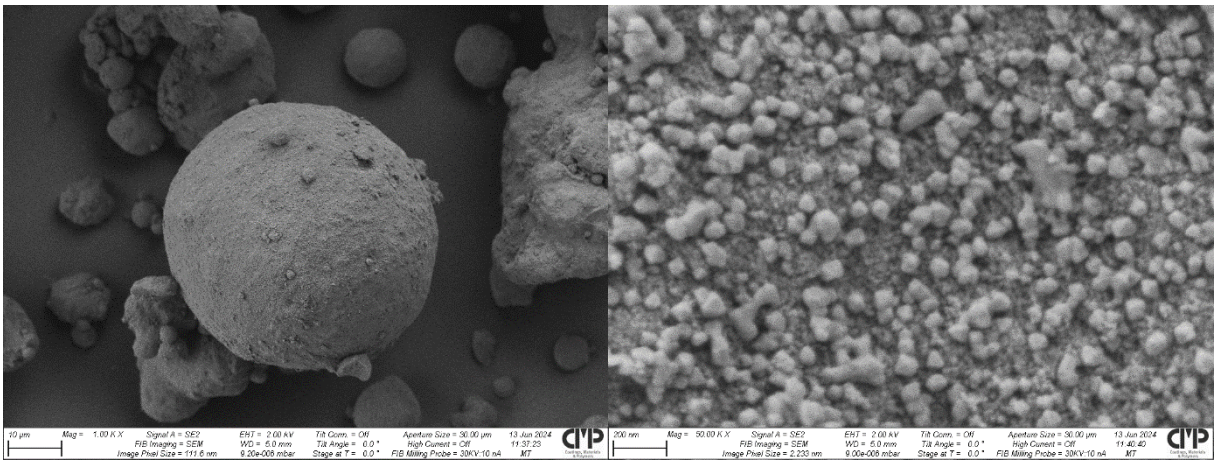


Figure S13: SEM pictures of SI10 in 1 000 fold (left) and 50 000 fold magnification (right).

XAS

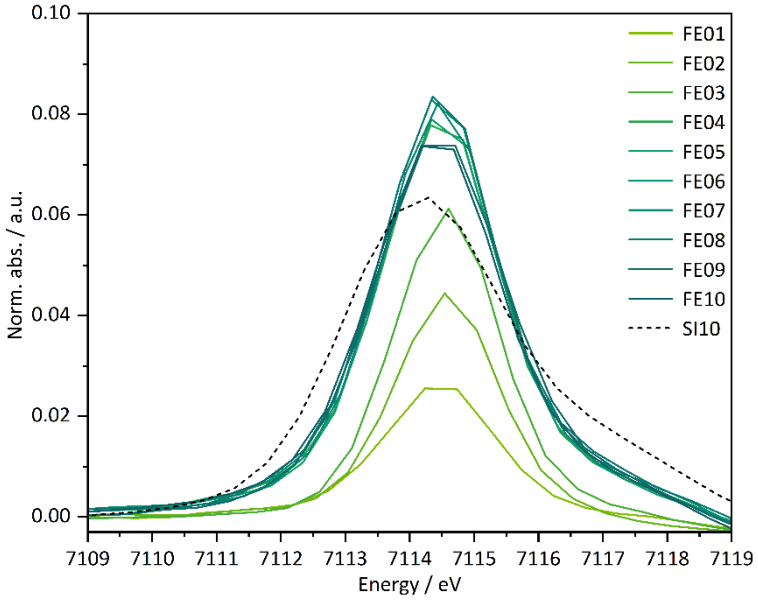


Figure S14: Baseline corrected pre-peaks of FE01 - FE10, SI10 and the α- and γ-Fe_2O_3 reference obtained from XANES spectra.

To compare the pre-peak-intensities and energies of the catalysts as detailed as possible, a Lorenzian-type curve was fitted to the spectra, subtracted and plotted in Figure S14.

Due to the fact, that the maximum of the SI10 prepeak is slightly shifted to lower energies compared to the FE catalyst spectra and in addition exhibits an asymmetric shape, a fit of two Gaussian-type functions was carried out for SI10 and in addition for α- and γ-Fe_2O_3, since these spectra as well show this behaviour as can be seen in Figure S15 to Figure S17.

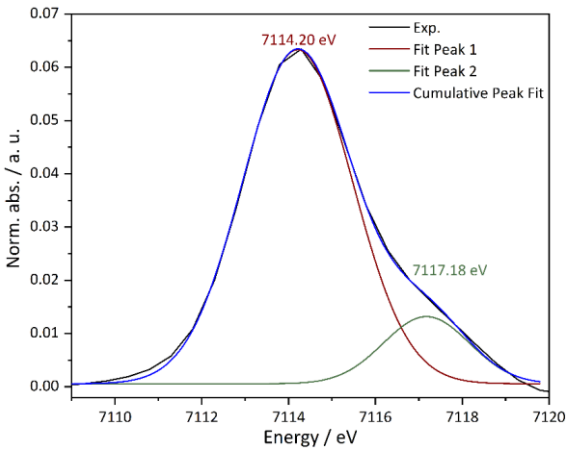


Figure S15: Pre-peak fit of SI10 using two Gaussian type functions.

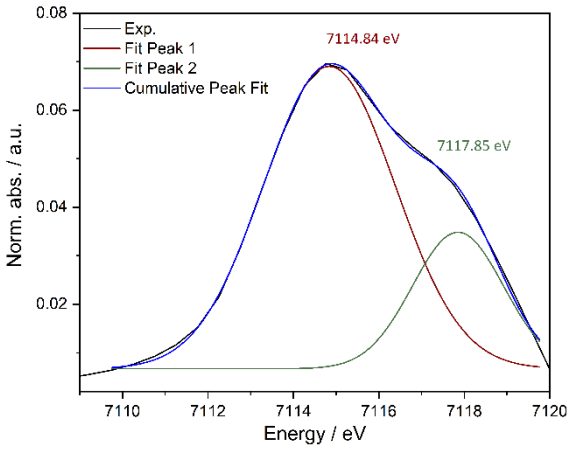


Figure S16: Pre-peak fit of α-Fe_2O_3 using two Gaussian type functions.

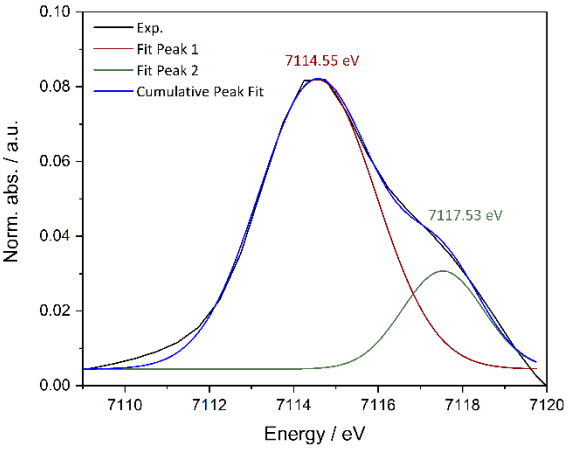


Figure S17: Pre-peak fit of γ-Fe_2O_3 using two Gaussian type functions.

Table S2: Pre-peak and edge positions of FE01 - FE10, SI10 and the α- and γ-Fe_2O_3 reference. Pre-peak positions were obtained by baseline correction of the XANES spectra followed by fit of one or two Gaussian type functions; edge positions were obtained as maximum in the first derivative of the spectrum (for more information see SI).

Catalyst	**Pre-peak [eV]**		**Edge position [eV]**
FE01	7114.46		7123.45
FE02	7114.57		7122.83
FE03	7114.57		7122.89
FE04	7114.49		7123.07
FE05	7114.48		7123.11
FE06	7114.47		7122.96
FE07	7114.48		7122.85
FE08	7114.47		7122.98
FE09	7114.49		7122.66
FE10	7114.42		7122.66
SI10	7114.20	7117.18	7125.72
α-Fe_2O_3	7114.84	7117.85	7125.11
γ-Fe_2O_3	7114.55	7117.53	7125.86

Table S3: Structural parameters obtained by EXAFS analysis of the catalysts FE01 - FE10, SI10 and the α- and γ-Fe_2O_3 reference; Abs = absorbing atom; Bs = backscattering atom; n(Bs) = number of backscattering atoms; r(Abs-Bs) = distance of absorbing to backscattering atom; σ = Debye-Waller-like factor; R = fit index; E_f = Fermi energy; Afac = amplitude reducing factor.

Catalyst	Abs-Bs	n(Bs)	r(Abs-Bs) [Å]	σ [$Å^{-1}$]	
FE01	Fe–O	0.1 ± 0.01	1.876 ± 0.018	0.002 ± 0.001	
	Fe–O	3.0 ± 0.15	1.923 ± 0.019	0.009 ± 0.001	**R** = 24.94 %
	Fe–O	3.1 ± 0.15	2.074 ± 0.020	0.023 ± 0.002	**E_f** = 1.649 eV
	Fe–Fe	0.4 ± 0.04	3.016 ± 0.030	0.008 ± 0.001	**Afac** =0.9477
	Fe–Al	5.7 ± 0.57	3.430 ± 0.034	0.025 ± 0.002	**n(Fe)/n(Al)** = 0.67
	Fe–Fe	3.4 ± 0.34	3.447 ± 0.034	0.024 ± 0.002	
FE02	Fe–O	0.2 ± 0.01	1.807 ± 0.018	0.002 ± 0.001	
	Fe–O	4.4 ± 0.22	1.954 ± 0.019	0.013 ± 0.001	**R** = 26.51 %
	Fe–O	2.1 ± 0.10	2.164 ± 0.021	0.024 ± 0.002	**E_f** = 1.160 eV
	Fe–Fe	0.3 ± 0.03	3.039 ± 0.030	0.002 ± 0.001	**Afac** = 0.9477
	Fe–Al	4.9 ± 0.49	3.441 ± 0.034	0.025 ± 0.002	**n(Fe)/n(Al)** = 0.71
	Fe–Fe	3.3 ± 0.33	3.457 ± 0.034	0.024 ± 0.002	
FE03	Fe–O	0.5 ± 0.02	1.836 ± 0.018	0.002 ± 0.001	
	Fe–O	3.7 ± 0.18	1.946 ± 0.019	0.010 ± 0.001	**R** = 22.14 %
	Fe–O	1.4 ± 0.07	2.134 ± 0.021	0.007 ± 0.001	**E_f** = 2.170 eV
	Fe–Fe	0.2 ± 0.02	3.053 ± 0.030	0.002 ± 0.001	**Afac** = 0.9477
	Fe–Al	4.6 ± 0.46	3.386 ± 0.033	0.024 ± 0.002	**n(Fe)/n(Al)** = 0.67
	Fe–Fe	2.9 ± 0.29	3.407 ± 0.034	0.025 ± 0.002	
FE04	Fe–O	0.9 ± 0.04	1.836 ± 0.018	0.004 ± 0.001	
	Fe–O	2.8 ± 0.14	1.946 ± 0.019	0.002 ± 0.001	**R** = 22.12 %
	Fe–O	1.7 ± 0.08	2.134 ± 0.021	0.002 ± 0.001	**E_f** = 1.934 eV
	Fe–Fe	0.4 ± 0.04	3.053 ± 0.030	0.025 ± 0.002	**Afac** = 0.9477
	Fe–Al	4.3 ± 0.43	3.386 ± 0.033	0.025 ± 0.002	**n(Fe)/n(Al)** = 0.63
	Fe–Fe	2.3 ± 0.23	3.407 ± 0.034	0.021 ± 0.002	
FE05	Fe–O	1.4 ± 0.07	1.803 ± 0.018	0.002 ± 0.001	
	Fe–O	3.2 ± 0.16	1.959 ± 0.019	0.004 ± 0.001	**R** = 32.88 %
	Fe–O	1.5 ± 0.07	2.128 ± 0.021	0.007 ± 0.001	**E_f** = 3.491 eV
	Fe–Fe	0.4 ± 0.03	3.075 ± 0.030	0.020 ± 0.002	**Afac** = 0.9477
	Fe–Al	4.4 ± 0.44	3.345 ± 0.034	0.025 ± 0.002	**n(Fe)/n(Al)** = 0.64
	Fe–Fe	2.4 ± 0.24	3.373 ± 0.037	0.025 ± 0.002	
FE06	Fe–O	1.3 ± 0.06	1.758 ± 0.017	0.002 ± 0.001	
	Fe–O	3.8 ± 0.19	1.944 ± 0.019	0.002 ± 0.001	**R** = 25.88 %
	Fe–O	1.4 ± 0.07	2.128 ± 0.021	0.002 ± 0.001	**E_f** = 3.917 eV
	Fe–Fe	0.3 ± 0.03	3.087 ± 0.030	0.005 ± 0.001	**Afac** = 0.9477
	Fe–Al	4.7 ± 0.47	3.318 ± 0.033	0.025 ± 0.002	**n(Fe)/n(Al)** = 0.57
	Fe–Fe	2.4 ± 0.24	3.342 ± 0.033	0.024 ± 0.002	

Catalyst	Abs-Bs	n(Bs)	r(Abs-Bs) [Å]	σ [$Å^{-1}$]	
FE07	Fe–O	1.4 ± 0.07	1.800 ± 0.018	0.002 ± 0.001	
	Fe–O	3.5 ± 0.17	1.960 ± 0.019	0.002 ± 0.001	**R** = 28.83 %
	Fe–O	1.7 ± 0.08	2.153 ± 0.021	0.002 ± 0.001	**E_f** = 2.651 eV
	Fe–Fe	0.6 ± 0.03	2.986 ± 0.029	0.025 ± 0.002	**Afac** = 0.9477
	Fe–Al	4.4 ± 0.44	3.383 ± 0.033	0.020 ± 0.002	**n(Fe)/n(Al)** = 0.80
	Fe–Fe	2.9 ± 0.29	3.404 ± 0.034	0.022 ± 0.002	
FE08	Fe–O	1.9 ± 0.09	1.825 ± 0.018	0.002 ± 0.001	
	Fe–O	3.0 ± 0.15	1.986 ± 0.019	0.002 ± 0.001	**R** = 25.58 %
	Fe–O	1.3 ± 0.06	2.188 ± 0.021	0.018 ± 0.001	**E_f** = 3.788 eV
	Fe–Fe	0.9 ± 0.09	3.093 ± 0.030	0.025 ± 0.002	**Afac** = 0.9477
	Fe–Al	5.5 ± 0.55	3.359 ± 0.033	0.025 ± 0.002	**n(Fe)/n(Al)** =0.85
	Fe–Fe	3.8 ± 0.38	3.377 ± 0.033	0.025 ± 0.002	
FE09	Fe–O	1.4 ± 0.07	1.841 ± 0.018	0.002 ± 0.001	
	Fe–O	2.5 ± 0.12	1.986 ± 0.019	0.004 ± 0.001	**R** = 25.24 %
	Fe–O	1.5 ± 0.07	2.146 ± 0.021	0.016 ± 0.001	**E_f** = 1.610 eV
	Fe–Fe	0.7 ± 0.07	3.032 ± 0.030	0.020 ± 0.002	**Afac** = 0.9477
	Fe–Al	4.2 ± 0.42	3.394 ± 0.033	0.023 ± 0.002	**n(Fe)/n(Al)** =0.86
	Fe–Fe	2.9 ± 0.29	3.405 ± 0.034	0.025 ± 0.002	
FE10	Fe–O	1.2 ± 0.06	1.829 ± 0.018	0.002 ± 0.001	
	Fe–O	3.0 ± 0.15	1.968 ± 0.019	0.005 ± 0.001	**R** = 25.64 %
	Fe–O	1.9 ± 0.09	2.152 ± 0.021	0.016 ± 0.001	**E_f** = 1.764 eV
	Fe–Fe	0.7 ± 0.07	3.014 ± 0.030	0.022 ± 0.002	**Afac** = 0.9477
	Fe–Al	3.7 ± 0.37	3.396 ± 0.033	0.025 ± 0.002	**n(Fe)/n(Al)** =0.86
	Fe–Fe	2.5 ± 0.25	3.416 ± 0.034	0.025 ± 0.002	
SI10	Fe–O	1.4 ± 0.07	1.803 ± 0.018	0.002 ± 0.001	
	Fe–O	3.2 ± 0.16	1.959 ± 0.019	0.004 ± 0.001	**R** = 32.88 %
	Fe–O	1.5 ± 0.07	2.128 ± 0.021	0.007 ± 0.001	**E_f** = 3.491 eV
	Fe–Fe	0.4 ± 0.03	3.075 ± 0.030	0.020 ± 0.002	**Afac** = 0.9477
	Fe–Al	4.4 ± 0.44	3.345 ± 0.034	0.025 ± 0.002	**n(Fe)/n(Al)** = 0.64
	Fe–Fe	2.4 ± 0.24	3.373 ± 0.037	0.025 ± 0.002	
α-Fe_2O_3	Fe–O	3.2 ± 0.16	1.961 ± 0.019	0.081 ± 0.008	**R** = 27.77 %
	Fe–O	3.3 ± 0.16	2.134 ± 0.021	0.110 ± 0.011	**Ef** = 2.584 eV
	Fe–Fe	6.3 ± 0.31	2.983 ± 0.029	0.112 ± 0.011	**Afac** = 0.9735
	Fe–Fe	2.9 ± 0.29	3.317 ± 0.033	0.112 ± 0.011	
	Fe–Fe	1.2 ± 0.12	3.706 ± 0.037	0.063 ± 0.006	
γ-Fe_2O_3	Fe–O	0.7 ± 0.03	1.868 ± 0.018	0.032 ± 0.003	**R** = 24.68 %
	Fe–O	4.8 ± 0.14	2.003 ± 0.020	0.105 ± 0.010	**Ef** = 3.112 eV
	Fe–Fe	4.4 ± 0.44	3.019 ± 0.030	0.112 ± 0.011	**Afac** = 0.8219
	Fe–Fe	2.1 ± 0.21	3.467 ± 0.034	0.087 ± 0.008	
	Fe–Fe	3.6 ± 0.36	5.128 ± 0.051	0.112 ± 0.011	

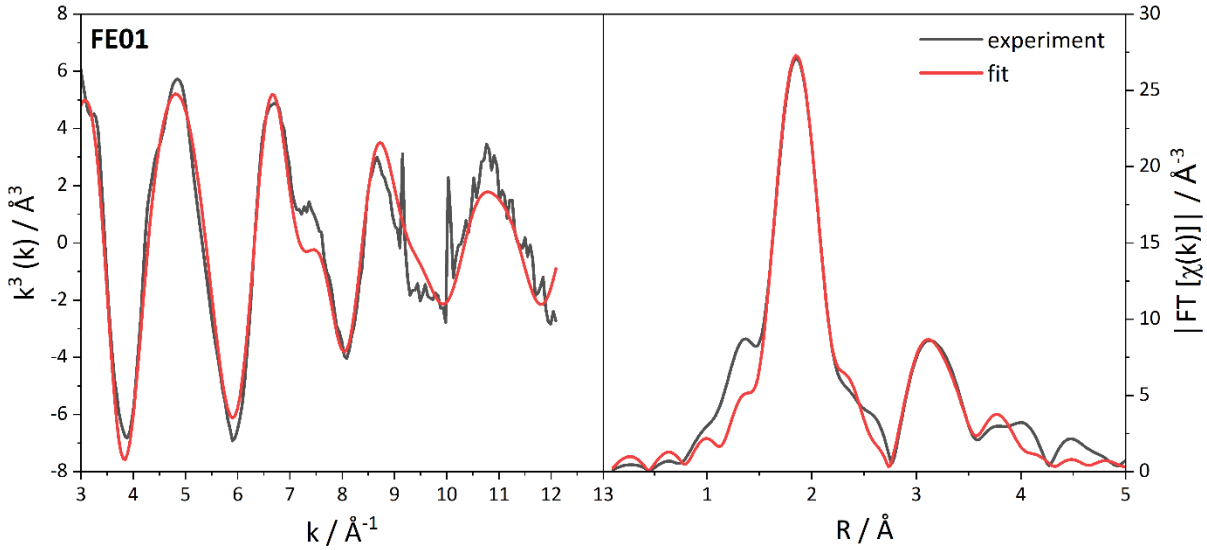


Figure S18: EXAFS fit of FE01 in k-space (left) and Fourier-transformed R-space (right).

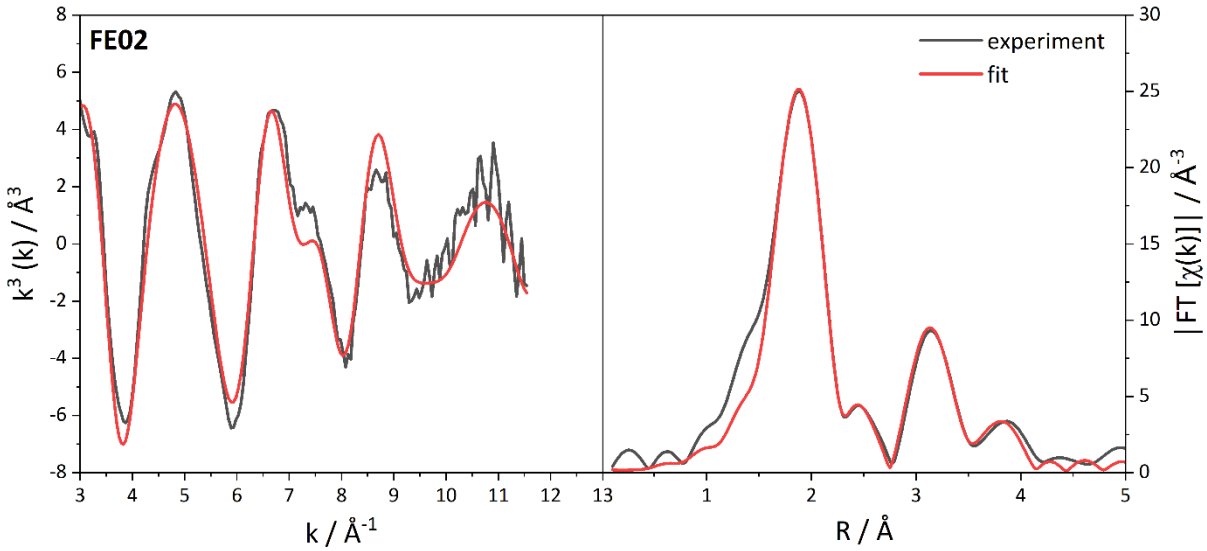


Figure S19: EXAFS fit of FE02 in k-space (left) and Fourier-transformed R-space (right).

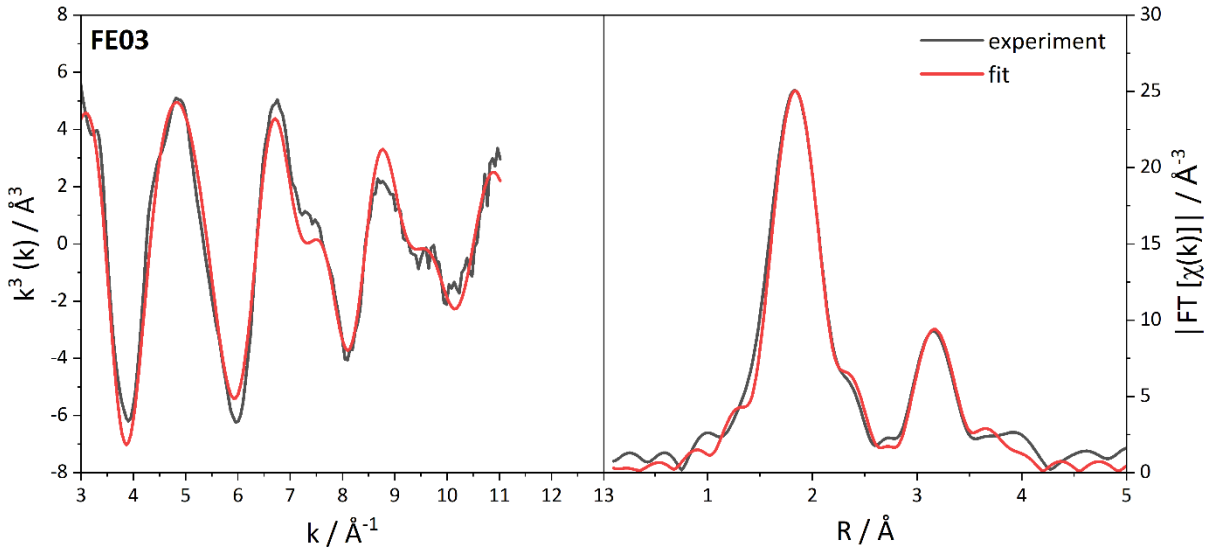


Figure S20: EXAFS fit of FE03 in k-space (left) and Fourier-transformed R-space (right).

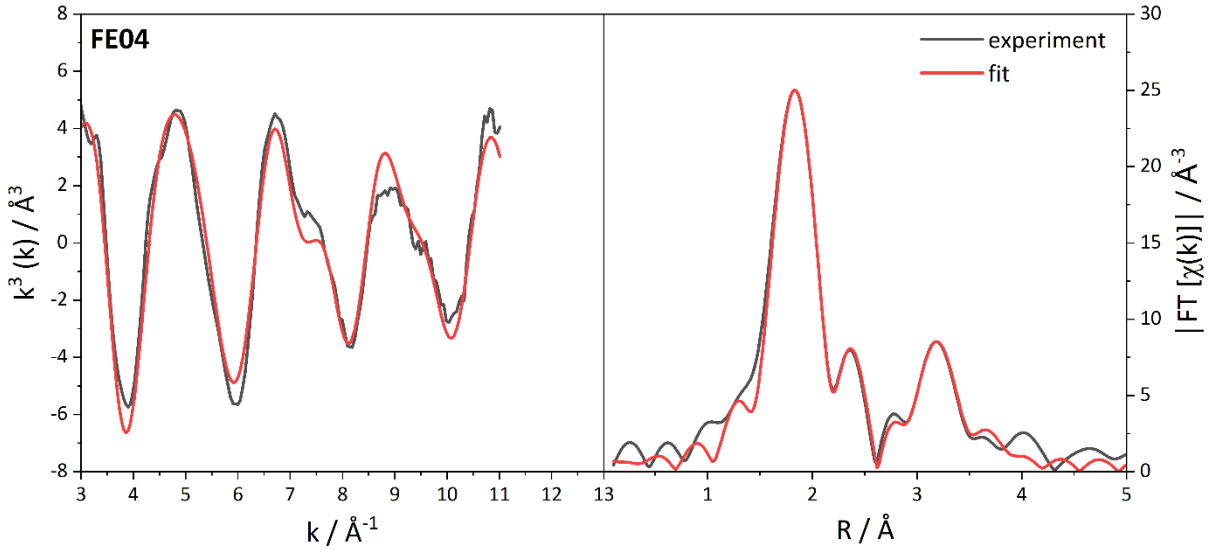


Figure S21: EXAFS fit of FE04 in k-space (left) and Fourier-transformed R-space (right).

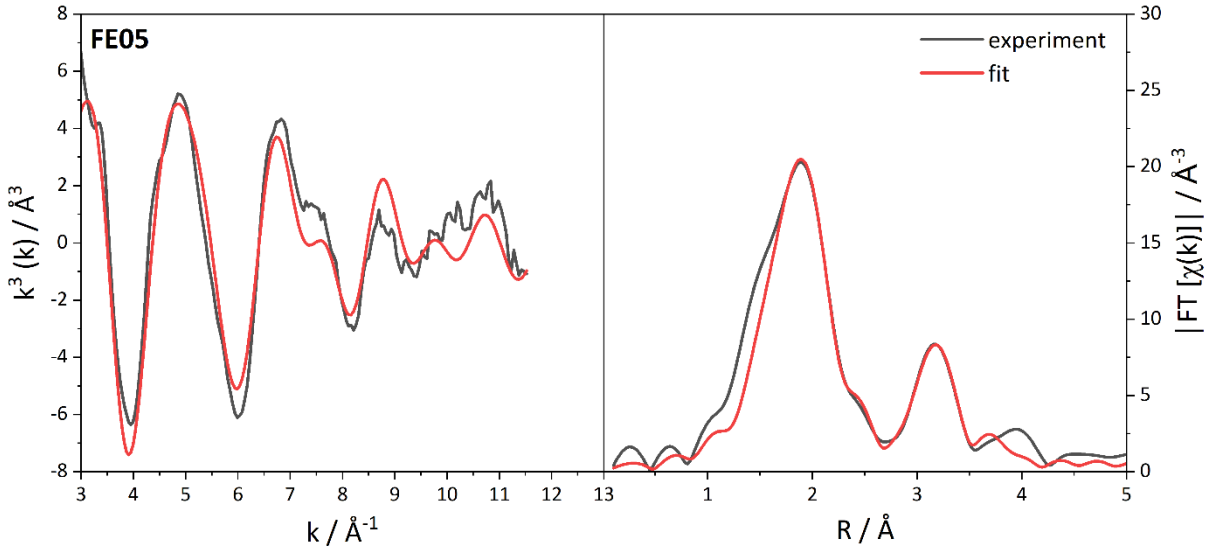


Figure S22: EXAFS fit of FE05 in k-space (left) and Fourier-transformed R-space (right).

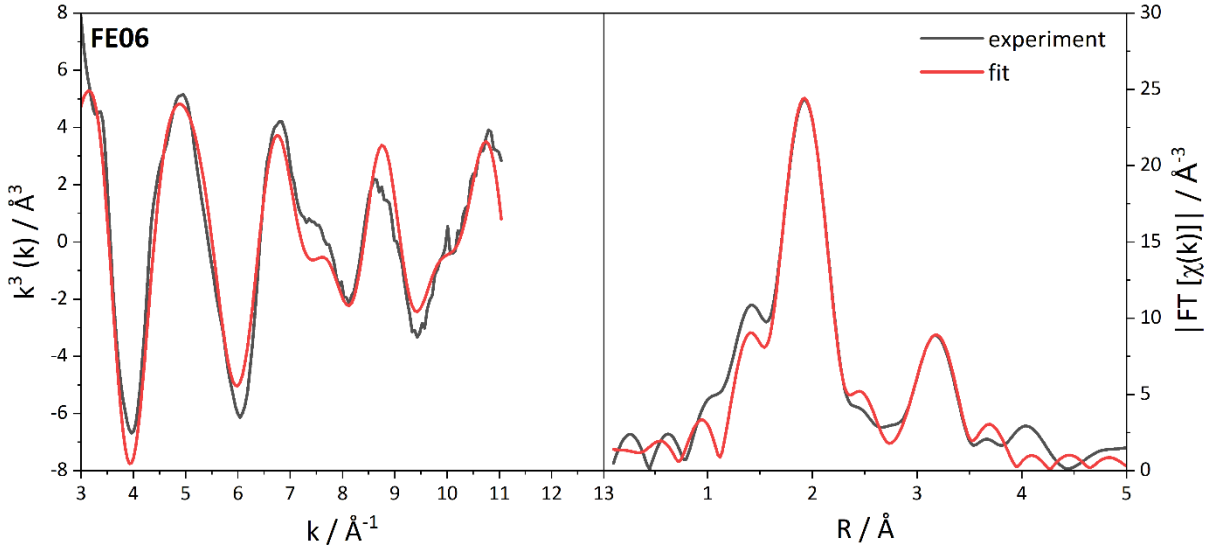


Figure S23: EXAFS fit of FE06 in k-space (left) and Fourier-transformed R-space (right).

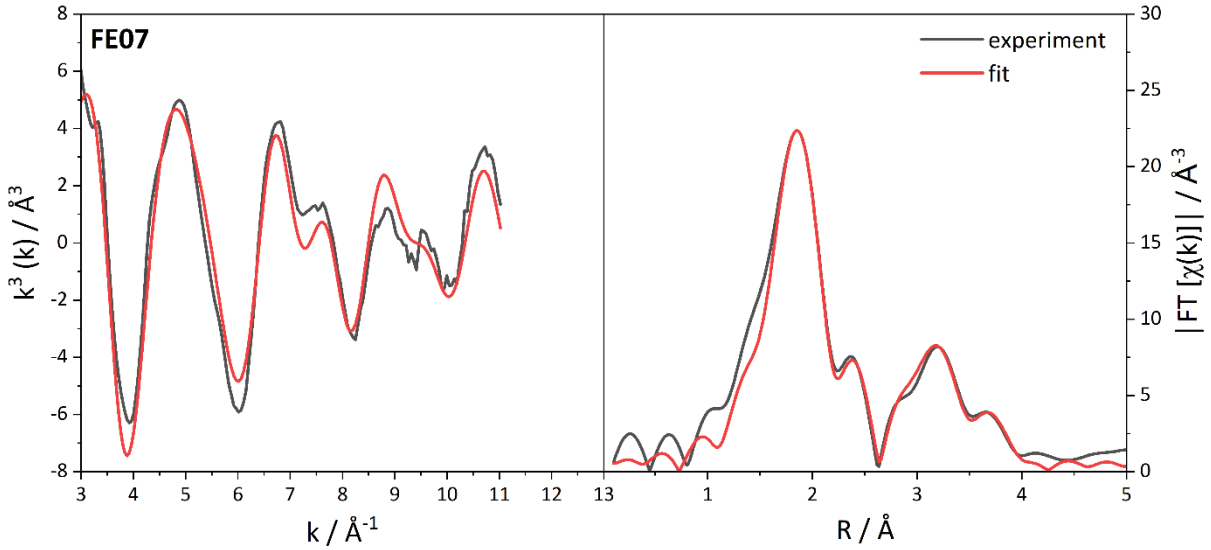


Figure S24: EXAFS fit of FE07 in k-space (left) and Fourier-transformed R-space (right).

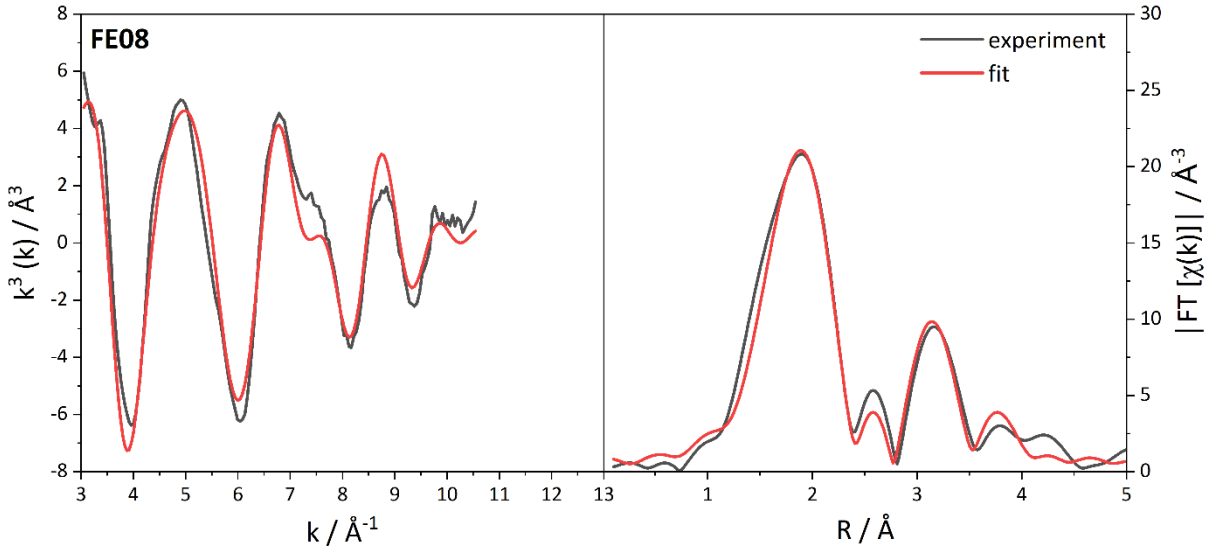


Figure S25: EXAFS fit of FE08 in k-space (left) and Fourier-transformed R-space (right).

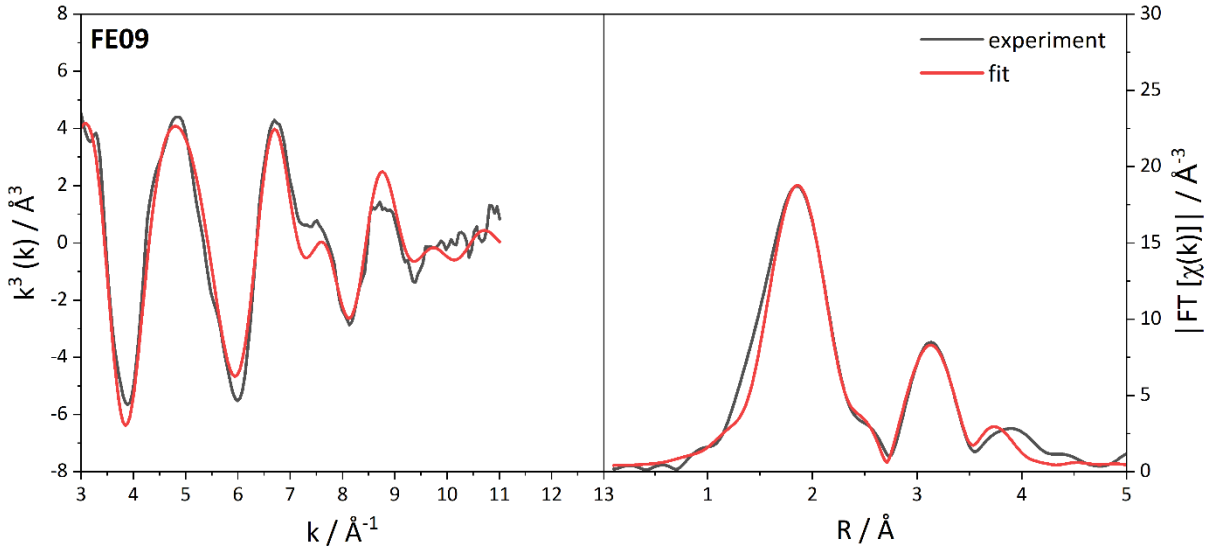


Figure S26: EXAFS fit of FE09 in k-space (left) and Fourier-transformed R-space (right).

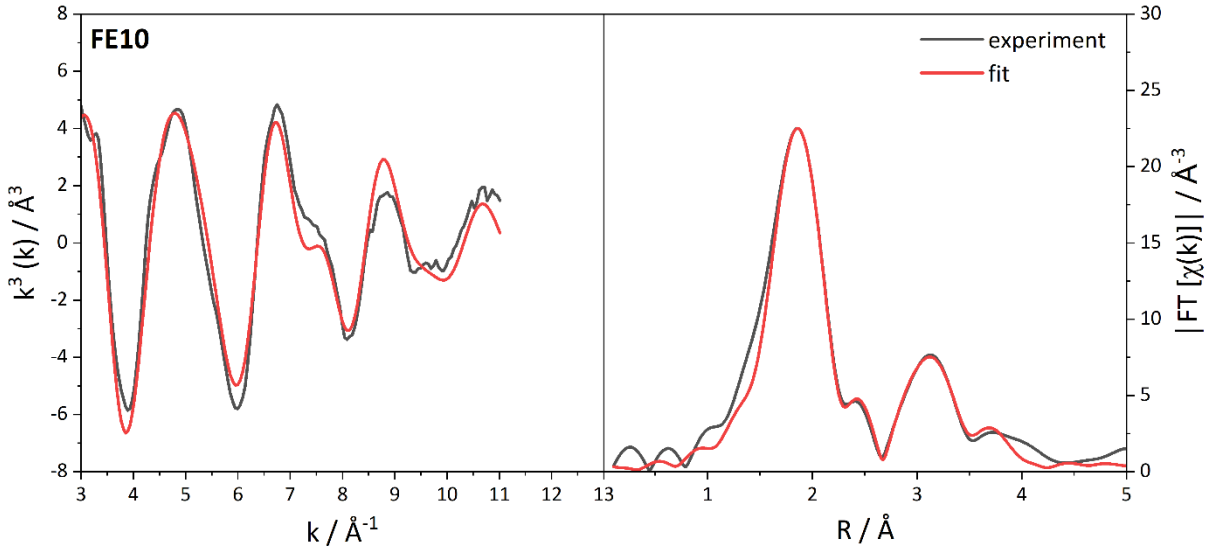


Figure S27: EXAFS fit of FE10 in k-space (left) and Fourier-transformed R-space (right).

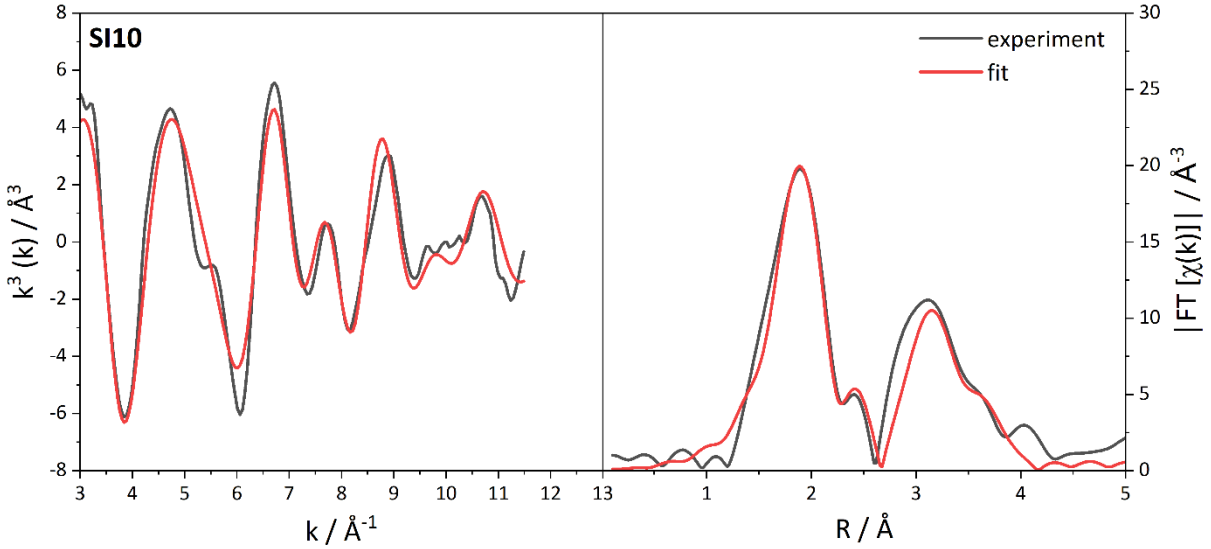


Figure S28: EXAFS fit of SI10 in k-space (left) and Fourier-transformed R-space (right).

Catalytic tests

In addition to the measurements during continious heating, static temperature experiments were carried out in 50 °C steps and 2 h per step between 150 and 400 °C. The results are shown in Figure S29. The catalysts with lower iron loadings, FE01 to FE05, show similar behaviour like in the continuous measurements: The conversion increases with loading. Interestingly, the activity of these catalysts stagnates between 250 and 300 °C, which is not detectable in the continuous measurements. A similar behaviour is recognizable for the higher loaded catalysts FE06 to FE08, but here the "activity plateau" is reached at lower temperatures between 200 and 250 °C. The catalysts with the highest loadings do not show a plateau at all. FE10 and the reference catalyst SI10 reveal very comparable activities at all temperatures, which are significantly higher than from the lower loaded catalysts – especially in the temperatures between 200 and 300 °C. FE09 shows a higher catalytic activity than the rest of the samples, with full conversion at 250 °C. A CO_2 yield of 100 % is only achieved by FE06 to FE10 and SI10 above 350 °C and at 400 °C by FE03 to FE05, while FE01 and FE02 do not reach the point of full conversion in this temperature range.

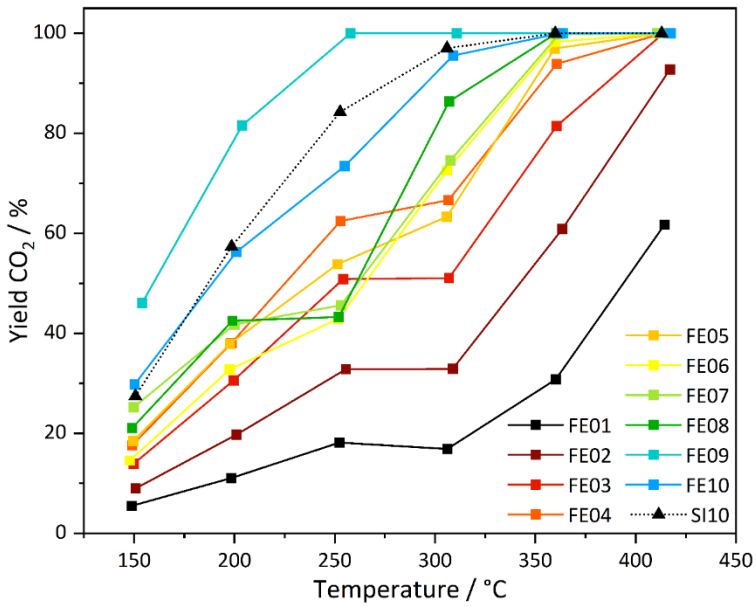


Figure S29: CO_2 yields of FE01 to FE10 and SI10 obtained from CO oxidation experiments at static temperatures.

The trends in the turnover frequencies from static measurements exhibit two maxima in the temperature range up to 300 °C for FE01 to FE04 and for FE09. FE08, FE10 and SI10 show comparably small values between 150 and 250 °C. At 400 °C the trend is clearest but mostly due to the fact, that except FE01 and FE02, all other catalysts reached full conversion. Throughout these measurements the reference catalyst shows TOFs comparable to Fe10.

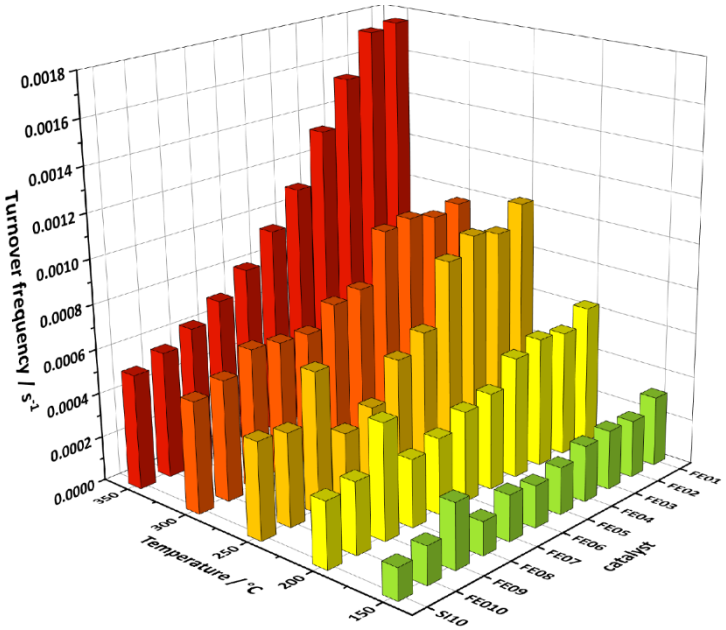


*Figure S30: TOFs of SI10 (marked with *) and FE01 - FE10, obtained from CO oxidation experiments at static temperatures of 150, 200, 250, 300 and 350 °C.*